JOURNAL OF SOLID STATE CHEMISTRY 103, 45–56 (1993)

From a Three- to a Four-Connected Net in Trimorphic CaPtSi at High Pressure

JÜRGEN EVERS, GILBERT OEHLINGER, KURT POLBORN, AND BERND SENDLINGER

Institut für Anorganische Chemie der Universität München, Meiserstrasse 1, D-8000 München 2, Federal Republic of Germany

Received March 26, 1992; in revised form July 27, 1992; accepted July 28, 1992

CaPtSi, midway between the Zintl phase $CaSi_2$ and the Laves phase $CaPt_2$, crystallizes at normal pressure in the LaIrSi-type structure, a derivative of the $SrSi_2$-type structure. Two quenchable polymorphs have been obtained from this phase in a belt apparatus at high pressures (3–4 GPa) and high temperatures (800–1100°C). The first high pressure polymorph (EuNiGe-type structure, *mP*12, $P2_1/n$, a = 588.9(1), b = 581.0(1), c = 724.3(1) pm, β = 109.25(1)°, Rietveld technique) is 7.3%, the second (TiNiSi-type structure, *oP*12, *Pnma*, a = 711.5(1), b = 433.6(1), c = 723.2(1), single crystal investigation) 11.6% more densely packed than the normal pressure phase. The denser packing is correlated with increases of coordination, bond distances, and metallic properties. The transformation from the LaIrSi- into the TiNiSi-type structure results in a change from a three-dimensional three-connected (Pt–Si: 230 pm) into a three-dimensional four-connected net (averaged Pt–Si: 254 pm). The phases of trimorphic CaPtSi show metallic behavior of the electrical resistivity and their magnetic susceptibility extends from diamagnetic (LaIrSi-type structure) to weakly paramagnetic (TiNiSi-type structure). A possible structural path from Zintl to Laves phases is discussed.

Introduction

The binary compounds MSi_2 (M = Ca,Eu,Sr,Ba), text-book examples of Zintl phases, have been studied structurally in four normal pressure (NP) and, up to 4 GPa, in four high pressure (HP) phases (*1*). The large differences in electronegativity between M and Si and the number of valence electrons have structure- and bonding-determining influence. In MSi_2, due to the Zintl concept, three-connected Si^- occurs in isolated tetrahedra, layers, and three-dimensional nets. The charge balance is maintained by M^{2+} ions. The binary compounds MT_2 (T = Pd,Pt), representatives of Laves phases, crystallize in the $MgCu_2$-type structure (*2, 3*) with polyhedra of high coordination numbers and efficient space filling. The ratio of radii is considered as the most determinative influence on bonding. It is well known that at HP coordination numbers, space filling, and metallic properties can be increased. To change structure and bonding in MSi_2 from Zintl to Laves phases at very high pressures (HP > 10 GPa) is, therefore, a challenge to HP chemistry.

The ternary compounds MTSi represent a quasi-binary section between Zintl phases MSi_2 on one and Laves phases MT_2 on the other side. Therefore ambivalent structural behavior is expected for these compounds.

0022-4596/93 $5.00

In the three homologous series *M*PdSi (*4*), *M*PtSi (*5*), and *M*PtGe (*6*), the LaIrSi-type structure (*7*) is very stable at NP and has been derived for 10 of 12 possible cases by single crystal or by Guinier powder investigations. Including LaIrSi, these compounds are isoelectronic with 16 valence electrons. The late transition metal and the metalloid build up a three-dimensional three-connected (3D3C) net (*8*) with bond distances between 230 and 245 pm. This structure is a derivative of the $SrSi_2$-type structure (*9*), stable for the Zintl phases $SrSi_2$ at NP and $BaSi_2$ at HP (*1*). However, the calcium compounds in these homologous series show interesting structural behavior. CaPtSi is stable in the LaIrSi-type structure, but CaPdSi and CaPtGe crystallize in two different structures where packing, coordination, bond distances, and metallic properties are increased.

A two-dimensional three-connected (2D3C) net with two additional contacts of low bond order is formed in the EuNiGe-type structure (*10*) of CaPdSi (*4*) and a three-dimensional four-connected (3D4C) net is found in the TiNiSi-type structure (*11*) of CaPtGe (*6*). The volume contraction in relation to the sum of the atomic volumina ($-\Delta V/V$) is much lower in CaPtSi (15.0%) than in CaPdSi (20.7%) and in CaPtGe (23.4%). Thus, CaPtSi, with lower packing and coordination than CaPdSi and CaPtGe, presents a very promising candidate for HP transformation.

This paper deals with synthesis and characterization of two HP polymorphs of CaPt Si, obtained at 3 GPa and 800°C and at 4 GPa and 1100°C in a belt apparatus. Both phases are quenchable to ambient conditions and then storable without retransformation into the NP phase. Their structural data have been derived by X-ray investigations of each powder on a computer-controlled Guinier diffractometer in the Rietveld technique (*12*) or of a single crystal on a four-circle diffractometer. The change of the metallic properties in trimorphic CaPtSi has been characterized by temperature-variable electrical resistivity (4-point technique) and magnetic susceptibility measurements (Faraday balance) on polycrystalline samples.

Experimental

In order to avoid contamination of the samples with ferromagnetic impurities, "clinical pure" conditions have been chosen for all preparative procedures. The NP phase of CaPtSi was prepared from ultra-high-vacuum-distilled calcium (*13*, *14*), electronic grade silicon (Wacker, Burghausen, Obb., FRG), and pure platinum (Degussa, FRG). At first, absence of ferromagnetic impurities in these materials was checked by plotting their magnetic susceptibility against the reciprocal magnetic field. Then weighed amounts of them (600–800 mg) were inductively melted in a water-cooled copper boat under purified argon. The copper boat can be transferred into a glove-box in which argon is continuously recirculated and purified. Due to the quasi-crucible-free melting, liquid CaPtSi does not wet the surface of the boat. Therefore contamination with impurities is limited and, after weighing, 1 : 1 : 1-composition of the ingot is easily controlled. By this preparative procedure the NP phase of CaPtSi, both pure and stoichiometric, is obtained. More experimental details are quoted elsewhere (*4*).

The HP phases of CaPtSi have been prepared in a belt apparatus in boron nitride crucibles. In order to prevent contamination, with ferromagnetic impurities, the boron nitride crucibles and graphite heaters were cleaned by boiling them in aqua regia. After washing and drying, absence of such impurities was tested as described above. Typical conditions in the belt apparatus were 3–4 GPa and 800–1200°C for 15 min and subsequent decompression after quenching to room temperature. Special

care was applied to scrape off the BN from the HP sample surface with instruments made of nonferromagnetic materials (e.g., molybdenum).

For X-ray powder experiments capillaries with very small diameter (0.15 mm) were used, since CaPtSi contains 74.1 wt% Pt and therefore absorbs X-rays strongly. Two thousand data points for the NP and 1500 data points for the HP phases were collected with Mo$K\alpha_1$ radiation (quartz-monochromator) at an increment of 0.02° (2Θ) (counting rate of 100 sec pro increment) on a computer-controlled Guinier diffractometer (G644, Huber-Diffraktionstechnik, Rimsting, Obb., Federal Republic of Germany). The 2Θ-range was between 8° and 48° for the NP polymorph CaPtSi I and between 6° and 36° for both HP polymorphs CaPtSi II and CaPtSi III. After correction of the data for absorption (*15*), the DICVOL method (*16*) was used for automatic indexing and then the Rietveld technique (*12*) for analyzing the structure. Details are summarized elsewhere (*4*).

Considerable effort was applied to prepare single crystals of both HP phases. However, in several experiments at 3 GPa and 800°C, only microcrystalline samples of the first HP polymorph were obtained, but at 4 GPa and 1100°C a single crystal (0.07 × 0.40 × 0.10 mm^3, without well developed faces) of the second HP polymorph was isolated. By Weißenberg photographs it was shown that CaPtSi III and CaPtGe (6) are isotypic. An Enraf-Nonius-CAD4 diffractometer with filtered Mo$K\alpha$ radiation was used for single crystal structure analysis. Nine hundred forty-seven reflections were measured in the Miller index range $h: \pm 7$, $k: \pm 4$, $l: 0 + 8$. After empirical absorption correction (μ = 667 cm^{-1}), two hundred forty-nine unique sets of observed reflections with $F \geq 3\sigma(F)$ (R_{int} = 9.65%) remained.

The electrical resistivity was measured in the temperature range between 300 and 540 K by the four-point technique on polycrystalline samples (NP phase, ingot of approximately 4 mm diameter and 8 mm length; HP-phases; cylindrical discs of 3 mm diameter and 1 mm height). The resistivity probe head consists of tungsten needles (diameter 0.5 mm) in square arrangement (distance 0.8 mm). The apparatus was calibrated with single-crystalline InSb (conductivity 220 Ω^{-1}cm^{-1} at room temperature). During several experiments typical values for the band gap of 0.20 ± 0.04 eV were derived, in agreement with the literature value of 0.236 eV (17).

The magnetic susceptibility of trimorphic CaPtSi was investigated on a Cahn microbalance by the Faraday technique on polycrystalline samples (approximately 100 mg). The magnetic field was varied betwen 4.9 and 8.4 kOe and the temperature between 77 and 600 K. Calibration was performed with high-purity mercury.

Results

Automatic indexing of the Guinier diffractograms of the high pressure phases showed that CaPtSi II is monoclinic (a = 588.9(1), b = 581.0(1), c = 724.3(1) pm, β = 109.25(1)°) and isotypic with CaPdSi (*4*) (EuNiGe-type structure (*10*)) and CaPtSi III is orthorhombic (a = 711.5(1), b = 433.6(1), c = 723.2(1) pm) and isotypic with CaPtGe (*6*) in the TiNiSi-type structure (*11*). The reliability indices F_{N20} (*18*) for the monoclinic and the orthorhombic phase are 10 and 9, respectively. Due to numerous overlapping reflections, these values are much lower than that for the cubic phase (F_{N20} = 29). With starting parameters of CaPtGe (*6*), structural calculations for the single crystal data on CaPtSi III were performed (SHELX program (*19*), isotropic refinement, 10 parameters, $R = R_w$ = 5.13%, R_G = 5.95%).

The crystallographic data for CaPtSi III are summarized in Table I. For purposes of

TABLE I

STRUCTURAL DATA FOR CUBIC (5) MONOCLINIC, AND ORTHORHOMBIC CaPtSi

Phase	Normal pressure CaPtSi I	High pressure CaPtSi II	High pressure CaPtSi III
Structure type	LaIrSi	EuNiGe	TiNiSi
Crystal system	cubic	monoclinic	orthorhombic
Space group	$P2_13$	$P2_1/n$	$Pnma$
Lattice parameters (pm,°)[a]	a = 632.0(5)	a = 588.9(1) b = 581.0(1) c = 724.3(1) β = 109.25(1)	a = 711.5(1) b = 433.6(1) c = 723.2(1)
Density (g/cm³)			
exp.	6.98	7.5	7.8
calc.	6.93(1)	7.47(1)	7.84(1)
Formula/cell	4	4	4
Positions[b]	(x, x, x)	(x, y, z)[c]	$(x, \frac{1}{4}, z)$
4 Ca	0.1276(6)	0.319 0.128 0.115	0.9958(9), 0.6885(9)
4 Pt	0.4189(1)	0.928(1) 0.108(1) 0.306(1)	0.1910(2), 0.0950(2)
4 Si	0.8345(9)	0.327 0.119 0.545	0.3256(13), 0.4169(13)
Therm. parameters U_{eq} (Å²)			
Ca	0.0090(9)		0.0038(14)
Pt	0.0162(2)		0.0038(5)
Si	0.0097(14)		0.0052(19)

[a] ESDs in parentheses.
[b] Position 4(a), space group $P2_13$; 4(a), $P2_1/n$; 4(c), $Pnma$.
[c] Ca and Si parameters from (*4*).

comparison crystallographic data of CaPtSi I, determined by an earlier single crystal investigation (*5*), are also presented. In addition, this table contains the results derived by the Rietveld technique for a powder of CaPtSi II. During the Rietveld refinement of this phase difficulties arose. First, the Guinier diffractogram of CaPtSi II had to be strongly corrected for absorption ($\mu \cdot r$ = 4) (*15*), resulting in correction factors of about 3 for reflections at low Θ-values. Second, Pt scatters X-rays about 30 times more strongly than Si and about 15 times more strongly than Ca. Thus, in Rietveld analysis of this phase, the positional parameters of Pt could be refined with sufficient accuracy, but not those of Ca and Si. For the latter, parameters determined by a single crystal investigation on isotypic and iso-valence-electronic CaPdSi (*4*) were used. They seem to be a good approximation for CaPtSi II since the cell volume of the Pd compound is only 0.4% lower than that of the Pt one and, furthermore, the metallic radius (*20*) of Pd (1.376 pm) is only 0.5% lower than that of Pt (1.383 pm). In Fig. 1 the Rietveld re-

FIG. 1. Rietveld refinement patterns for trimorphic CaPtSi: increment 0.02° (2Θ), counting rate per increment of 100 sec. The observed Guinier diffractogram is indicated by a solid line, the calculated by a broken line overlying it. Positions for possible reflections are marked by vertical lines. The difference plot between the observed and the calculated diffractograms is shown by the lower curve. (a) cubic phase I, 2Θ range 8–48°, R_p = 8.21%; (b) monoclinic phase II, 2Θ range 6°–36°, R_p = 10.74%; (c) orthorhombic phase III, 2Θ range 6°–36°, R_p = 9.70%.

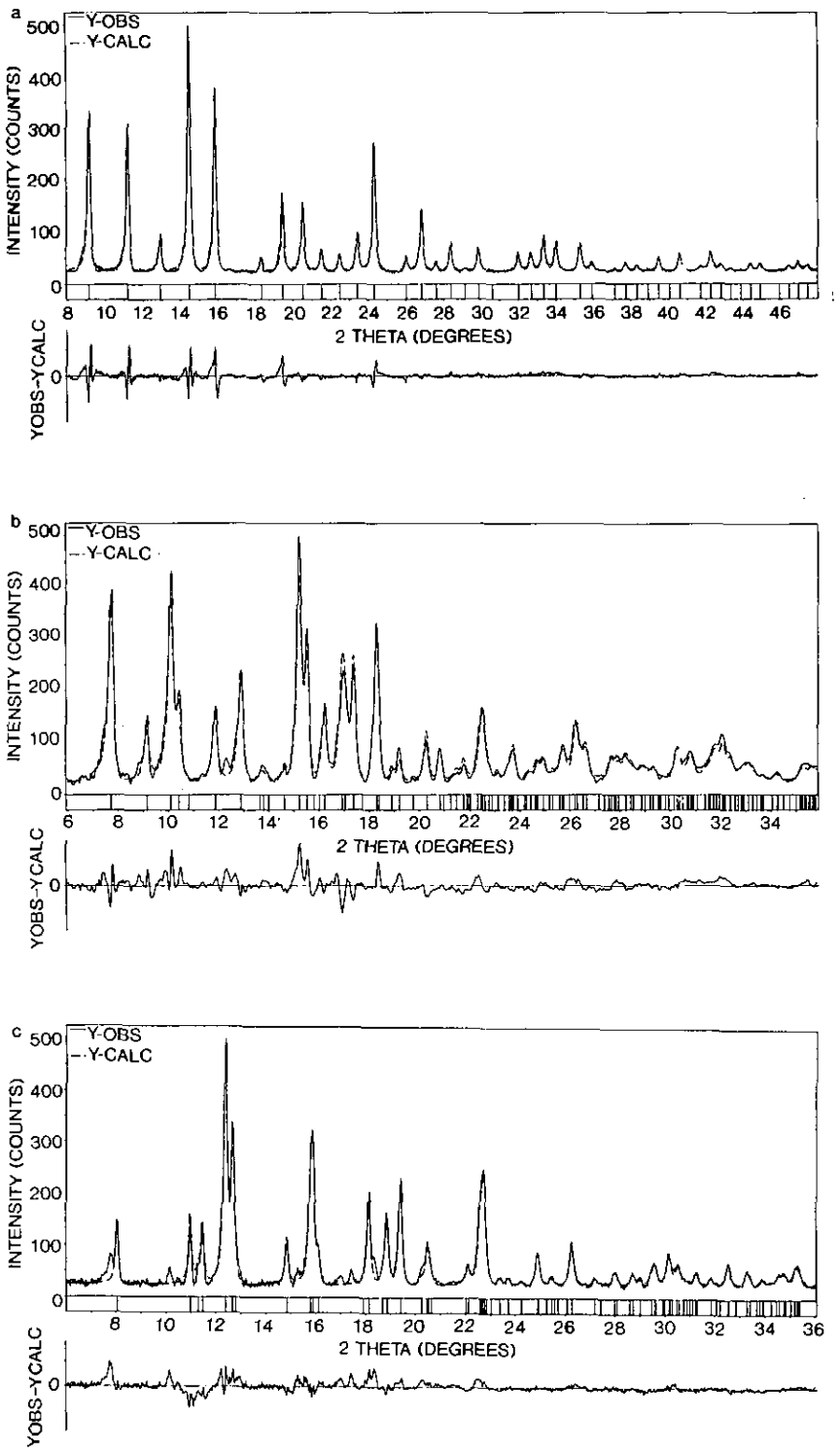
a
Y-OBS
Y-CALC
INTENSITY (COUNTS)
2 THETA (DEGREES)
YOBS-YCALC
b
Y-OBS
Y-CALC
INTENSITY (COUNTS)
2 THETA (DEGREES)
YOBS-YCALC
c
Y-OBS
Y-CALC
INTENSITY (COUNTS)
2 THETA (DEGREES)
YOBS-YCALC

TABLE II

NUMBER OF NEIGHBORS, BOND DISTANCES (pm), AND BOND ANGLES (°) FOR CUBIC (5), MONOCLINIC, AND ORTHORHOMBIC CaPtSi[a]

Cubic		Monoclinic		Orthorhombic	
Pt—3 Si 229.7(5)	Si—3 Pt 229.7(5)	Pt—1 Si 239(2)	Si—1 Pt 239(2)	Pt—1 Si 251.7(10)	Si—1 Pt 251.7(10)
		—1 Si 242(2)	—1 Pt 242(2)	—2 Si 252.4(10)	—2 Pt 252.4(10)
		—1 Si 250(2)	—1 Pt 250(2)	—1 Si 260.1(10)	—1 Pt 260.1(10)
		—1 Pt 294(1)	—1 Si 271(3)		
Ca—1 Si 320.8(11)	Ca—3 Pt 316.9(6)	Ca—1 Pt 295(2)	Ca—1 Si 301(3)	Ca—2 Si 300.7(12)	Ca—1 Pt 298.4(7)
—3 Si 320.9(11)	—1 Pt 318.8(6)	—1 Pt 306(2)	—1 Si 309(3)	—1 Si 306.0(12)	—2 Pt 298.6(7)
—3 Si 365.0(13)	—3 Pt 370.8(7)	—1 Pt 313(2)	—1 Si 310(3)	—1 Si 310.0(12)	—2 Pt 318.2(7)
		—1 Pt 322(2)	—1 Si 314(3)	—2 Si 324.2(12)	—1 Pt 325.1(7)
		—1 Pt 333(2)	—1 Si 319(3)		
		—1 Pt 339(2)	—1 Si 352(3)		
Ca—6 Ca 387.1(3)		Ca—1 Ca 345(3)		Ca—2 Ca 348.4(11)	
		—2 Ca 374(3)		—2 Ca 366.7(11)	
		—1 Ca 387(3)			
$Pt^{Si}Pt$ 118.5(1) (3×)		$Pt^{Si}Pt$ 121(2)	$Si^{Pt}Si$ 132(2)	$Pt^{Si}Pt$ 93.7(7) 2×, 110.5(7)	
		92(2)	119(2)	117.0(7) 2×, 118.4(7)	
$Si^{Pt}Si$ 117.9(1) (3×)		73(2)	107(2)	$Si^{Pt}Si$ 86.4(7) 2×, 114.3(7)	
				119.3(7) 2×, 118.4(7)	

[a] ESDs in parentheses.

finement patterns for trimorphic CaPtSi are shown and in Table II the number of neighbors, the bond distances (pm), and the bond angles (°) are summarized.

In Table III the results of the electrical measurements for trimorphic CaPtSi are presented. Their specific electrical resistivities are in the order of $10^{-4}\ \Omega \cdot$ cm at room temperature; their positive temperature coefficients indicate metallic behaviour. Figure 2 shows the variation of the specific electrical resistivity for CaPtSi I in the temperature range between 300 and 540 K.

In Table IV the masses and the molar magnetic susceptibilities at room temperature are summarized. A correction for diamagnetic contributions was not applied. The susceptibilities show only a weak temperature dependence in the range between 80 and 600 K. In Fig. 3 the molar magnetic susceptibilities at room temperature are plotted as a function of the reciprocal magnetic field. The horizontal graphs obtained for the three polymorphs of CaPtSi indicate the absence of ferromagnetic impurities. By

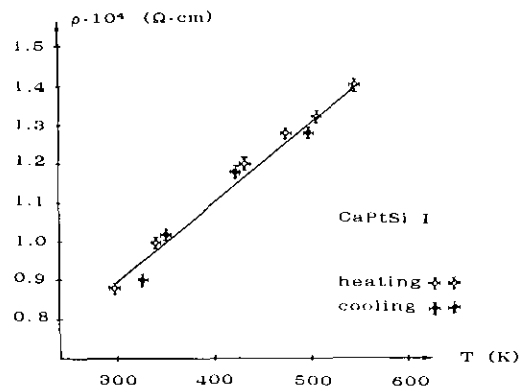

FIG. 2. Specific electrical resistivity for CaPtSi I in the temperature range between 300 and 540 K.

TABLE III

SPECIFIC ELECTRICAL RESISTIVITY ρ (*at* 20°C) AND ITS TEMPERATURE COEFFICIENT $d\rho/dT$ FOR TRIMORPHIC CaPtSi

	$\rho_{20°C}$ ($\Omega \cdot$ cm)	$d\rho/dT$ ($\Omega \cdot$ cm $\cdot$ deg^{-1})
CaPtSi I	0.9×10^{-4}	2.0×10^{-7}
CaPtSi II	10^{-4}	10^{-7}
CaPtSi III	10^{-4}	10^{-7}

TABLE IV

MASS AND MOLAR SUSCEPTIBILITIES AT ROOM TEMPERATURE FOR TRIMORPHIC CaPtSi

	$\chi_{g,20°C} \cdot 10^6$ (e.m.u./g)	$\chi_{M,20°C} \cdot 10^6$ (e.m.u./mole)
CaPtSi I	−0.30(1)	−79(3)
CaPtSi II	−0.14(1)	−37(3)
CaPtSi III	+0.04(1)	+11(3)

inspection of this figure it is obvious that diamagnetism decreases in the series from CaPtSi I to CaPtSi III. CaPtSi I and CaPtSi II are diamagnetic ($-79(3) \cdot 10^{-6}$, $-37(3) \cdot 10^{-6}$ in e.m.u./mole, respectively), but CaPtSi III is weakly paramagnetic ($+11(3) \cdot 10^{-6}$ e.m.u./mole, Table IV).

Discussion

As stated in the previous section, CaPtSi crystallizes up to 4 GPa and 1100°C in three different structures. At ambient conditions the cubic phase I with the LaIrSi-type structure (*7*) is stable; at 3 GPa and 800°C the monoclinic phase II with the EuNiGe-type structure (*10*) and at 4 GPa and 1100°C the orthorhombic phase III with the TiNiSi-type structure (*11*) is stable (Table I).

In the cubic phase I, platinum and silicon form a three-dimensional three-connected (3D3C) net in an ordered arrangement. From a Zintl viewpoint, the electropositive calcium (Pauling electronegativity $EN_{Ca} = 1.0$) donates two valence electrons to the more electronegative platinum ($EN_{Pt} = 2.2$) and silicon ($EN_{Si} = 1.8$), resulting in negative charges on the three-connected atoms: $(PtSi)^{2-}$. Cations Ca^{2+} fill the large cavities of the structure. In the 3D3C net of the binary Zintl phases $SrSi_2$(NP) (*9*) and $BaSi_2$(HP) (*1*) (space group $P4_332$), three-connected Si^- form flat trigonal pyramids with a four-membered repeat-unit. The top of such a flat pyramid is only about 35 pm higher than the three base atoms. In the ternary phase CaPtSi I, the net contains two types of trigonal pyramids, with either Pt or Si in the top site and with bases of either three Si or three Pt, respectively. Since a base site of one type of pyramid is also the top site of the other, the repeat unit is here six-membered and consists of 3 Pt and 3 Si. The bonds within the net are equidistant (229.7(5) pm, 3×, Table II), but the bond angles differ slightly ($Si^{Pt}Si$: 117.9(1)°, $Pt^{Si}Pt$: 118.5(1)°).

Platinum and silicon are arranged in two-fold helices (space group $P2_13$, Table I). By interlocking them, slightly distorted four-fold "helices" of uniform chirality are obtained. Two bonds of the three-connected atoms are found within such a fourfold "helix"; the third is used for the connection with adjacent ones. This connection is performed alternatively in two dimensions, creating in this way a three-dimensional net. For the positional parameter $x_{Pt} = \frac{3}{8}$ and $x_{Si} = \frac{7}{8}$ the ideal arrangement of the net is obtained which, projects two-dimensionally as a 4.8^2-net. In such a semiregular net, each three-connected atom is a member of one square and two octagons. Figure 4(a) shows the atomic arrangement in CaPtSi and the relation of the distorted 3D3C net with

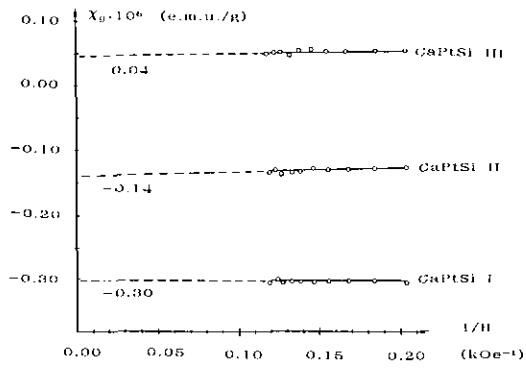

FIG. 3. Mass susceptibilities for trimorphic CaPtSi at room temperature as a function of reciprocal magnetic field.

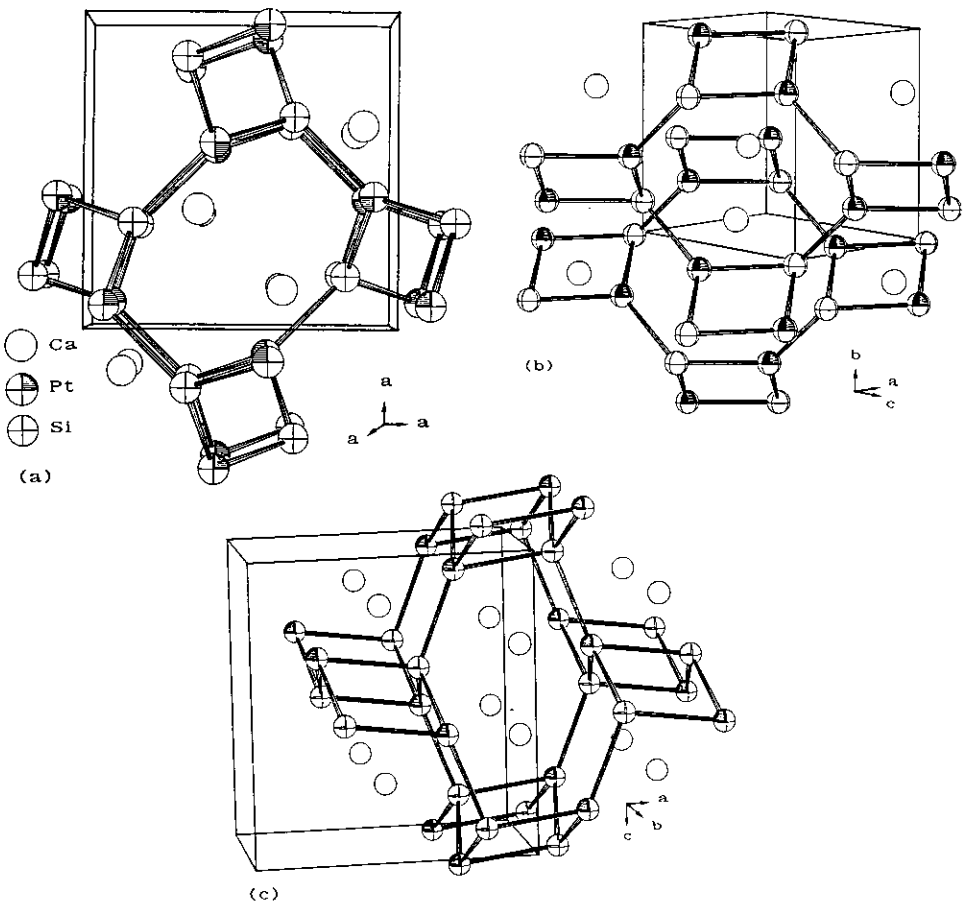

FIG. 4. Structural arrangements in trimorphic CaPtSi with relation to 4.8^2-nets:
(a) cubic phase I,
(b) monoclinic phase II,
(c) orthorhombic phase III.

x_{Pt} = 0.4189(1) and x_{Si} = 0.8345(9) (Table I) to a 4.8^2-net. Additional structural details have been given elsewhere (*5*).

In the monoclinic phase II (EuNiGe-type structure (*10*)) platinum and silicon form an ordered two-dimensional three-connected (2D3C) net with calcium lying between the layers. Also here the repeat unit consists of six members and two types of distorted trigonal pyramids as described above, but of lower symmetry than in phase I. For each type of pyramid, there are three different bond angles ($Si^{Pt}Si$: 132, 119, 107°; $Pt^{Si}Pt$: 121, 92, 73°; ESDs: 2°, Table II)). Bond distances within the net are also different (239, 242, 250 pm; ESDs: 2 pm). In addition, two longer contacts are found (Si–Si: 271(3), Pt–Pt: 294(1) pm) with Pauling bond orders of only 0.4 and 0.2, respectively.

Also here platinum and silicon are arranged in twofold helices (space group $P2_1/n$, Table I). Due to a center of symmetry, interlocking of them leads to distorted fourfold "helices" of alternating chirality. Two bonds are used within such a "helix"; the third is used for connection with adja-

cent ones, but in this case only in one dimension. In this way, puckered layers are created which contain three-connected Pt and Si in a distorted 4.8^2-arrangement. The layers are shifted in relation to each other in the $(10\bar{1})$-plane, achieving identity after three layers at $3 \cdot 524 = 1574$ pm. In Fig. 4(b) the atomic arrangement of CaPtSi II and its relation to a 4.8^2-net are shown.

In the orthorhombic phase III (TiNiSi-type structure (*11*)), platinum and silicon are arranged in an ordered three-dimensional four-connected (3D4C) net. It consists also of two types of trigonal pyramids, with either Pt or Si in the top site. Understanding of this net is easier if puckered three-connected layers in 4.8^2-arrangement are formed as in CaPtSi II (Fig. 4(b), but with uniform layer sequence. If the layers are brought together so that the interlayer distance is $b_{orth} = 433.6(1)$ pm, each top-site of a pyramid achieves one additional bond to the top site of one other type of pyramid. Now a 3D4C net is created, which consists of distorted tetrahedra of two types. The bond distances within such tetrahedra differ (251.7, 252.4 (2×), 260.1 pm; ESDs: 1.0 pm, Table II); so do the bond angles ($Pt^{Si}Pt$: 93.7 (2×), 110.5, 117.0 (2×), 118.4°; $Si^{Pt}Si$: 86.4 (2×), 114.3, 119.3 (2×), 118.4°; ESDs: 0.7°). Figure 4(c) shows the atomic arrangement of CaPtSi III and the relation of the 3D4C net to a 4.8^2-net.

If the 3D3C net of CaPtSi I is transformed into the 3D4C net of CaPtSi III, the increase from three- to fourfold Pt : Si coordination is correlated with an elongation of Pt–Si bond distances. In the cubic phase I the bond distance is 229.7(5) pm; in the orthorhombic it is 254 pm (averaged, Table II). For the 2D3C net of CaPtSi II an intermediate value of 243 pm (averaged) is derived, although in this case coordination is difficult to evaluate precisely. Although Pt–Si bond distances within the net of the HP phases are enlongated, they nevertheless achieve higher densities. The monoclinic phase is 7.3% and the orthorhombic 11.6% more densely packed than the cubic NP phase. These values must be correlated with increases in Ca : Pt(Si) coordination as well. Astonishingly, this is not evident at first sight. If one counts only the number of neighbors of the first coordination sphere, the calcium atoms in CaPtSi I are surrounded by seven Pt- and seven Si-neighbors between 317 and 371 pm. But in the HP polymorphs CaPtSi II and CaPtSi III, the calcium atoms have only six Pt- and six Si-neighbors between 295 and 352 pm (Table II). In order to clear up this discrepancy, the numbers of Ca-, Pt-, and Si-neighbors and also their sum within a sphere of 1200 pm around the calcium atoms are summarized in Table V. In CaPtSi I now 354 total Ca-, Pt-, and Si-neighbors are counted, in CaPtSi II 372, and in CaPtSi III 396. At this distance the increase in the number of neighbors is 5.1% for the transformation CaPtSi(I–II) and 11.9% for CaPtSi(I–III). Much better agreement with the density increases is achieved if the sphere for counting neighbors is sufficiently enlarged.

TABLE V

NUMBER OF Ca-, Pt-, AND Si-NEIGHBORS AND THEIR SUM WITHIN A SPHERE OF 1200 pm AROUND THE CALCIUM ATOMS FOR THE THREE PHASES OF CaPtSi

	Calcium Neighbors			
	Ca	Pt	Si	Total
CaPtSi I	116	119	119	354
CaPtSi II	119	126	127	372
CaPtSi III	142	127	127	396

In HP phases, in addition to the increases of packing, density, bond distances, and coordination numbers, often a more metallic state with regard to physical properties is approached. Inspection of Table III shows that the three phases of CaPtSi have specific

electrical resistivities at room temperature on the order of $10^{-4}\ \Omega \cdot$ cm with a positive (metallic) temperature coefficient. Unfortunately, for small polycrystalline discs of the HP polymorphs (diameter, 3 mm; height, 1 mm), it is not an easy job to evaluate their gradation in electrical resistivities. However, such a gradation is found for the magnetic susceptibilities (Table IV). Phase I with the 3D3C net is diamagnetic, phase III with the 3D4C net is weakly paramagnetic, with an intermediate magnetic susceptibility for the monoclinic phase II. Variation of temperature shows that the magnetic susceptibilities are nearly independent of this parameter, excluding the presence of unpaired *d*-electrons in the three phases of CaPtSi. Then paramagnetism must result here from conduction electrons being less present in phase I, but more in phase III. Therefore, the metallic state seems to increase from phase I via phase II to phase III.

In the course of analyzing the stability of various three-connected nets, Zheng and Hoffman (*21*) have calculated the density of states (DOS) for the 3D3C net of the LaIrSi-type structure. However, it was not the purpose of their paper to give sufficient details of the DOS near the Fermi level to derive the electronic properties of compounds with such a structure. For the two other structures of CaPtSi polymorphs, information regarding DOS is not available up to now. Thus, only a very small understanding of the electronic properties of trimorphic CaPtSi from a more "molecular" view is just possible. Due to the Zintl concept, in binary $CaSi_2$(NP) (10-valence-electron system) with layers of three-connected silicon (*1*), there are five valence electrons on each Si. Simply, three of them are located in three σ-bonds; two are located in a nonbonding pair and would cause semiconductivity here. Because of band overlapping, $CaSi_2$ (NP)—with metallic behavior of the electrical resistivity (*22*)—is a diamagnetic semimetal. In ternary CaPtSi I (16e) with a three-connected Pt–Si net, platinum has six valence electrons more than silicon (formal electron count $Pt^0: d^8s^2$, $Si^0: s^2p^2$). Now there are three electron "pairs" more on Pt than on Si which do not contribute to paramagnetism in phase I. Due to such a "localization" of valence electrons, CaPtSi I—with metallic behavior of the electrical resistivity (Table III)—is a diamagnetic semimetal (perhaps as well as LaIrSi with also 16e). In the 3D4C net of CaPtSi III each Pt and Si atom contributes one additional valence electron for the fourth Pt–Si bond. Thus, one unpaired valence electron remains on each of them: phase III is a paramagnetic metal. Only very weak fourth bonds (bond orders 0.4 and 0.2) are formed in phase II. Therefore the increase of paramagnetism is here much lower: phase II is midway between a semimetal and a metal. Nevertheless, for a quantitative discussion, detailed information on the DOS near the Fermi level is required.

As described above, the metallic properties in CaPtSi can be increased by HP transformation. Interestingly, in the homologous series CaPt*X* (*X* = Si, Ge, Sn, Pb) this is achieved at NP, if one uses as alloying component for the ternary compounds instead of Si the more metallic elements Ge, Sn, and Pb. Then CaPtGe, CaPtSn, and CaPtPb crystallize in the 3D4C net of the TiNiSi-type structure even at NP, as do CaPdSn and CaPdPb. The lattice parameters, derived by the Rietveld technique, are summarized and compared with CaPtSi III in Table VI. CaPtGe and CaPtSn have also been characterized by single-crystal investigations on a four-circle diffractometer. The averaged bond distances in the 3D4C net increase from 254 pm in CaPtSi III to 260 pm in CaPtGe (*6*) and then to 272 pm in CaPtSn (*23*). Unfortunately, it was not possible to evaluate precisely the large bond distances in the nets of the two lead compounds, since

TABLE VI

LATTICE PARAMETERS[a] FOR CaPtGe, CaPtSn, CaPtPb, CaPdSn, AND CaPdPb OBTAINED AT NP WITH TiNiSi-TYPE STRUCTURE IN COMPARISON WITH CaPtSi III

Phase	Condition	a(pm)	b(pm)	c(pm)
CaPtSi III	HP	711.5(1)	433.6(1)	723.2(1)
CaPtGe	NP	716.9(2)	440.9(2)	743.8(2)
CaPtSn	NP	731.4(2)	457.4(2)	793.0(2)
CaPtPb	NP	729.7(5)	464.3(5)	816.9(5)
CaPdSn	NP	729.3(2)	457.2(2)	805.0(2)
CaPdPb	NP	730.6(5)	465.8(5)	822.6(5)

[a] ESDs in parentheses.

here isolation of suitable single crystals has failed up to now.

The high pressure structural behavior of the CaPtX series represents an interesting analogue to that of the homologous main-group-IV series C, Si, Ge, and Sn. The diamond structure is thermodynamically stable at NP for Si, Ge, and Sn, but only at HP for the first main-group-IV element C. Furthermore, the β-Sn structure is obtained for Sn at NP, but for Ge, Si, and C with increasing HP. If there existed a comparable dependence in the CaPdX and in the CaPtX series also, one could expect a transformation of the 3D4C nets in CaPdPb and in CaPtPb at much lower HP than in CaPdSi and in Ca PtSi. Indeed, a quenchable HP phase with ZrNiAl-type structure (*24*, *25*) has been obtained from CaPdPb at 4 GPa and 1000°C (a = 783.4(5), c = 388.2(3) pm (*23*)). This phase, CaPdPb II, is 1.8% more densely packed than the 3D4C net of the TiNiSi-type structure in CaPdPb I. Both structures of ternary CaPdPb are derivatives of binary ones: the TiNiSi-type structure is derived from the $CeCu_2$-type structure (*26*) and the ZrNiAl-type structure from the Fe_2P-type structure (*27*). Interestingly, for the ZrNiAl-type structure HP transformation into the $MgCu_2$-type structure has been studied. For compounds of the homologous series RCuAl (R = Sm to Lu) the ZrNiAl-type structure is stable at NP, but the $MgCu_2$-type structure has been evaluated at HP (*28*).

Therefore, it would be very interesting to characterize the gradual change in structure and properties in the homologous CaPdX and CaPtX series (X = Si, Ge, Sn, Pb) at increasing HP > 10 GPa. It can be assumed that a structural path of gradually higher packing, density, coordination, and metallic properties is terminated at the $MgCu_2$-type structure, perhaps easier to achieve for the ternary phases CaPdPb and CaPtPb, but more difficult for the binary $CaSi_2$. For the last, such a structural path runs from the $CaSi_2$-type structure at NP to the α-$ThSi_2$-type structure at 4 GPa (*1*) and then possibly—as a challenge to chemistry at very HP, via $CeCu_2$- and Fe_2P- to the $MgCu_2$-type structure of the Laves phase.

Acknowledgment

Thanks are due to the Fonds der Chemischen Industrie.

References

1. J. EVERS, *J. Solid State Chem.* **24,** 199 (1978); **28,** 369 (1979); **32,** 77 (1980).
2. E. A. WOOD AND V. B. COMPTON, *Acta Crystallogr.* **11,** 429 (1958).
3. A. IANDELLI AND A. PALENZONA, *J. Less-Common Met.* **38,** 1 (1974); **80,** 71 (1981).
4. J. EVERS, G. OEHLINGER, K. POLBORN, AND B. SENDLINGER, *J. Solid State Chem.* **91,** 250 (1991).
5. J. EVERS AND G. OEHLINGER, *J. Solid State Chem.* **62,** 133 (1986).
6. J. EVERS, G. OEHLINGER, K. POLBORN, AND B. SENDLINGER, *J. Alloys*, in press.
7. K. KLEPP AND E. PARTHÉ, *Acta Crystallogr. B* **38,** 1541 (1982).
8. A. F. WELLS, "Three-Dimensional Nets and Polyhedra," Wiley, New York, 1977.
9. K. H. JANZON, H. SCHÄFER, AND A. WEISS, *Angew. Chem.* **77,** 258 (1965).
10. B. D. ONISKOVETS, V. K. BELSKII, V. K. PECH-

ARSKI, AND O. I. BODAK, *Kristallografiya* **32,** 888 (1987). [*Soviet Phys. Crystallogr.* **32,** 522 (1987)].
11. C. B. SHOEMAKER AND D. P. SHOEMAKER, *Acta Crystallogr.* **18,** 900 (1965).
12. D. B. WILES AND R. A. YOUNG, *J. Appl. Crystallogr.* **14,** 149 (1981).
13. B. SENDLINGER, Diplomarbeit, Universität München (1989).
14. J. EVERS, G. OEHLINGER, C. PROBST, M. SCHMIDT, P. SCHRAMEL, AND A. WEISS, *J. Less-Comm. Met.* **81,** 15 (1981).
15. K. SAGEL, "Tabellen zur Röntgenstrukturanalyse," Springer-Verlag, Berlin (1958).
16. D. LOUER AND R. VARGAS, *J. Appl. Crystallogr.* **15,** 542 (1982).
17. O. MADELUNG, "Grundlagen der Halbleiterphysik," Heidelberger Taschenbücher, p. 176, Springer-Verlag, Berlin (1970).
18. G. S. SMITH AND R. L. SNYDER, *J. Appl. Crystallogr.* **12,** 60 (1979).
19. G. SHELDRICK, "SHELX," (program for the solution of crystal structures), University of Göttingen, D-3400 Göttingen.
20. W. B. PEARSON, "The Crystal Chemistry of Metals and Alloys," Wiley–Interscience, New York/London (1972).
21. C. ZHENG AND R. HOFFMANN, *Inorg. Chem.* **28,** 1074 (1989).
22. J. EVERS AND A. WEISS, *Mater. Res. Bull.* **9,** 549 (1974).
23. J. EVERS, G. OEHLINGER, K. POLBORN, AND B. SENDLINGER, to be published.
24. B. Y. KOTUR, O. I. BODAK, AND O. Y. KOTUR, *Dopov. Akad. Nauk Ukr. RSR Ser. A Fiz. Mat. Tekh. Nauki* **8,** 80 (1980).
25. E. HOVESTREYDT, N. ENGEL, K. KLEPP, AND E. PARTHÉ, *J. Less-Common Met.* **85,** 247 (1982).
26. A. C. LARSON, *Acta Crystallogr.* **14,** 73 (1961).
27. S. RUNDQUIST, *Acta Chem. Scand.* **13,** 425 (1959).
28. A. V.TSYASHCHENKO AND L. N. FOMICHEVA, *J. Less-Comm. Met.* **134,** L13 (1987).